https://dx.doi.org/10.1016/j.apenergy.2019.05.072

Performance characteristics of a passive direct ethylene glycol fuel cell with hydrogen peroxide as oxidant

Zhefei Pan[1], Yanding Bi[1], Liang An*

Department of Mechanical Engineering, The Hong Kong Polytechnic University, Hung Hom, Kowloon, Hong Kong SAR, China.

[1] Equal contribution.

*Corresponding author.

Email: liang.an@polyu.edu.hk (L. An)

Abstract

A passive direct ethylene glycol fuel cell is proposed and tested, which does not contain external liquid pumps, gas blowers/compressors or any other auxiliary device. Therefore, comparing to the active fuel cells, the volumetric energy density is improved. In this work, ethylene glycol in alkaline solution is employed as fuel in this fuel cell, while hydrogen peroxide in acid solution is employed as oxidant, and a cation exchange membrane is employed to transport cations. The theoretical voltage of this type of fuel cell is as high as 2.47 V, which exhibits a promising potential in practical applications. The operating conditions can influence the performance of this fuel cell system, including species concentrations in both fuel and oxidant, thicknesses of membranes, and operating temperatures. In addition, the open-circuit voltage and the peak power density of this fuel cell are as high as 1.58 V and 65.8 mW cm^{-2} at 60°C, respectively. Comparing to a fuel cell system with a similar setting but using oxygen as oxidant, the higher voltage output and power output are attributed to the easier and faster reduction reaction of hydrogen peroxide, which makes contributions to the impressive performance improvement of this fuel cell.

Moreover, the effect of the released heat caused by the hydrogen peroxide self-decomposition to the cell performance is studied as well.

Keywords: Passive fuel cells; Direct ethylene glycol fuel cell; Hydrogen peroxide; Operating parameters; Power density; Hydrogen peroxide self-decomposition

1. Introduction

Fuel cells have attracted great research interest as a promising power source in the last decades, which is mainly attributed to their simple design [1,2], high efficiency [3,4], low emissions [5,6] as well as quick refueling [7,8]. Three common fuels, i.e., hydrogen [9], methanol [10], and ethanol [11], are widely used in proton exchange membrane fuel cells (PEMFCs) [12] as well as anion exchange membrane fuel cells (AEMFCs) [13,14]. Among them, the widespread application of hydrogen is required to address the production, transport, and storage of hydrogen [15,16]. As for methanol, the fuel cell performance is severely degraded under long-term operation due to the severe crossover of methanol and the poisonousness of catalyst derivatives [17]. Ethanol, a C_2 fuel, has a main final oxidation product of acetic acid. When the system works at a temperature lower than 60°C, the electron transfer rate is low (33%) [16,18]. Recently, another fuel option, ethylene glycol (EG), has attracted wide attention due to its excellent properties [19,20], including the theoretical energy capacity of 4.8 Ah mL^{-1}, the boiling point of 198°C [21], and the electron transfer rate of 80%, which is suitable for mobile, stationary and portable devices [22,23]. Zhu et al. [20] synthesized hollow $Ag_{44}Pt_{56}$ nanotube bundles for ethylene glycol oxidation reaction (EGOR). To improve the electrocatalytic activity, Shi et al. [21] and Huang et al. [22] prepared three-dimensional nitrogen-doped reduced graphene oxide hydrogels anchored PtPd alloyed nanoparticles and PtCu alloyed nanocages with highly open structures via one-pot solvothermal method, respectively. Pan et al. [23] developed a mathematical modeling of direct ethylene glycol fuel cells using hydrogen peroxide as oxidant incorporating the effect of the competitive adsorption. An et al. [24] reported an alkaline direct ethylene glycol fuel cell (DEGFC) with a maximum peak power density of 67 mW cm^{-2} at 60°C, which was attributed to the alkaline media enhancing the kinetics of both the EGOR and oxygen reduction reaction (ORR). The anion exchange membrane (AEM) and non-platinum catalysts

are adopted in this fuel cell. Afterwards, an alkali-doped polybenzimidazole membrane was used to replace the AEM, which allows the system to be operated at high temperatures [25]. As a result, the maximum peak power densities of this fuel cell were 80 mW cm^{-2} at 60ºC and 112 mW cm^{-2} at 90ºC, respectively. Air or pure oxygen is usually used as oxidant on the cathode [25, 26]. It is necessary to compress the pure oxygen to store it in tanks. However, by doing so, the system becomes bulkier, and the complexity and potential risks are increased [27]. In addition, although the air breathing design is compact and light, one major issue is the carbonate problem in alkaline fuel cells, referring to the phenomenon that CO_2 in the ambient air reacts with hydroxide ions to produce carbonates [1]. The active sites in the cathode are covered by the precipitated carbonates, which causes the sluggish ORR kinetics [28]. At the same time, the pores and channels are blocked in the cathode, which increases the mass transport resistance of oxygen [29]. In addition, the air breathing design is not applicable with the absence of air, such as underwater and outer space. Recently, extensive research has been conducted on replacing air or pure oxygen with hydrogen peroxide as oxidant [30,31]. There are three intrinsic superiorities by using hydrogen peroxide: (1) the theoretical voltage will experience a substantial increase; (2) comparing to the four-electron transfer process of ORR, only two electrons are transferred in the hydrogen peroxide reduction reaction (HPRR), which reduces the activation loss; and (3) the water flooding will be avoided due to the aqueous state of hydrogen peroxide [32]. Pan et al. [33] designed and tested an active DEGFC using hydrogen peroxide as oxidant. Comparing to the DEGFC using oxygen as oxidant, the cell performance is elevated significantly. The open-circuit voltage (OCV) is improved by 62.1% to 1.41 V, while the peak power density is elevated by 20.8% to 80.9 mW cm^{-2} at 60ºC. However, the active electrolyte delivery system requires auxiliary equipment, making the system more complicated and heavier.

In this work, a passive DEGFC using hydrogen peroxide as oxidant is developed, which avoids the usage of auxiliary devices. The proposed fuel cell system is structurally compact, no parasitic loss in power, and can operate under low-temperature, which makes it a suitable choice for portable electronic devices [34]. Because of the simpler and more compact structures, the volumetric energy density and the design flexibility are elevated significantly. This fuel cell consists of a palladium-based anode, a cation exchange membrane (CEM), and a gold-based cathode. The theoretical voltage of this system is 2.47 V. When operating at 60°C, it exhibits a practical OCV of 1.58V, and a peak power density of 65.8 mW cm^{-2}. In addition, the effect of operating conditions and the heat released from the H_2O_2 self-decomposition on the cell performance are also investigated.

2. Working principle

As demonstrated in Figure 1 (a), the passive fuel cell is formed in a symmetric manner, which consists a diffusion layer (DL) and a catalyst layer (CL) in both anode and cathode, and a CEM between the two electrodes. The anolyte is injected into the anode reservoir. Under the driving force of the concentration gradient, it transports through the DL to the CL in the anode. The EGOR occurs on the anode CL where EG reacts with hydroxide ions to produce electrons, oxalate and water as shown below [18]:

$$C_2H_6O_2 + 10OH^- \rightarrow (COO^-)_2 + 8e^- + 8H_2O \qquad E_{EGOR}=-0.69\ V \qquad (1)$$

Through the external circuit, the electrons produced by the EGOR are transferred from the anode to the cathode. In the cathode, the hydrogen peroxide, protons, and electrons participate in the hydrogen peroxide reduction reaction (HPRR) and water is produced as shown in the following equation [35]:

$$4H_2O_2 + 8H^+ + 8e^- \rightarrow 8H_2O \qquad E_{HPRR}=1.78\ V \qquad (2)$$

At the same time, the internal ionic circuit is formed by the potassium ions transferring from the anode to cathode. Therefore, the EGOR and HPRR reactions can be combined to form the overall reaction of this fuel cell, which is shown as follows:

$$C_2H_6O_2+4H_2O_2+8H^++10OH^-\rightarrow(COO^-)_2+16H_2O \quad E=2.47\ V \qquad (3)$$

As shown in Equation (3), the theoretical voltage of this passive fuel cell is as high as 2.47 V. However, due to the presence of activation loss, ohmic loss, and concentration loss, the actual voltage will experience a huge decrease.

3. Experimental

3.1. Preparation of membrane electrode assembly

The membrane electrode assembly (MEA) consists of a pair of home-made electrodes that serve as the anode and the cathode, as well as CEMs with different thicknesses, including 30 μm (N211), 60 μm (N212), and 120 μm (N115). The thicknesses of the dry CEMs were measured by a vernier caliper. The electrodes have an active area of 2.0 cm × 2.0 cm. The Pd/C anode was prepared based on the method reported somewhere else [36]. Firstly, the catalyst ink was prepared. 30 wt.% Pd/C (Sigma-Aldrich Co., USA) was mixed with 5 wt.% Nafion (Fuel Cell Store, USA), which serves as the binder, and ethanol, which serves as the solvent. The ink was then dispersed in ultrasonic bath for 20 minutes. Subsequently, it was sprayed onto the backing layer, i.e., carbon cloth (Hesen, China). The catalyst loading on the anode was 1.0 mg_{Pd} cm^{-2}. The Au/C cathode was prepared by the same method except that the ink used in the cathode was made by 60 wt.% Au/C (Premetek Co., USA) with 15 wt.% Nafion and ethanol. The catalyst loading of cathode was 2.66 mg_{Au} cm^{-2}. To obtain the CEMs, original Nafion membranes were cut to the designed shape (3.00 cm × 3.00 cm) and immersed in 2.5 M KOH solution at 80ºC for 1h [36]. Then, the treated membranes were rinsed by washing it in DI water for several times and stored in DI water before the assembly of this fuel cell.

3.2. Fuel cell setup and instrumentation

As shown in Figure 1 (b), an end plate, a heating plate and a current collector are added to both sides of the MEA to form the whole fuel cell system, in which end plates and heating plates are made of 1Cr18Ni9Ti stainless steel and current collectors are made of 316L stainless steel. Several polytetrafluoroethylene (PTFE) gaskets are placed between each component of the fuel cell to avoid the leakage. The heating plates serve as the solution reservoir as well. As shown in Figure 1 (b), two holes are drilled on the top surface of the heating plate. One is a perforative hole designed for injecting the anolyte or catholyte, and the other is not perforative and designed for placing the heating rod. The current collectors are manufactured by laser cutting with 25 holes in the center part with a diameter of 3.2 mm. The holes allow the fuel and oxidant to diffuse from the reservoir to the anode and cathode.

An Arbin BT2000 (Arbin instrument Inc.) is utilized to control the discharging process of this passive fuel cell and measure the polarization curves. Meanwhile, the built-in function of the Arbin BT2000 is utilized to measure the internal resistance of this fuel cell. In addition, to examine the fuel cell performance with specific operating temperatures, two electrical heating rods are inserted into the holes on the heating plates and two thermocouples and a dual-channel temperature controller are used to control the anode and cathode temperatures.

4. Results and discussion

4.1. Advantages of passive fuel cells

Compared to active fuel cells using external pumps or other auxiliary devices for fuel and oxidant supply, the advantages of passive fuel cells can be concluded as follows: (1) The passive fuel cells have much simpler and more compact structures, which increases both the volumetric energy density and the design flexibility of the fuel cell system [37]; (2) The passive fuel cells eliminate the electricity consumed by the added pumps, blowers, and compressors, which can be regarded as parasitic energy losses [38]; and (3) Especially for

portable and mobile electrical devices, using passive fuel cells is more favorable than the active fuel cells due to the simplicity of diffusion and natural-convection reactant delivery [39]. Although the passive fuel cells yield lower power output than dose the active fuel cells, they are still considered as a promising power source for applications in future electronic devices. For instance, the research and development of passive fuel cells have been conducted by several giant electronic companies, including Toshiba, Samsung, NEC, etc. [40]. Radically different from our previous work, hence, we develop and demonstrate a passive fuel cell using EG and hydrogen peroxide as fuel and oxidant, respectively. It is a promising power source to be applied underwater and outer space where oxygen is insufficient.

4.2. Characterization of catalyst layers

Figure 2 (a) and (b) show the scanning electron microscope (SEM) images of the anode CL and the cathode CL, respectively. It is seen from Figure 2 (a) that the carbon fibers were decorated with carbon supported Pd nanoparticles. Since the loading is as low as 1.0 mg cm^{-2}, partial carbon fibers are bare, indicating that further increasing the catalyst loading may promote the fuel cell performance. As shown in Figure 2 (b), the carbon supported Au nanoparticles entirely covered the carbon fibers and were uniformly distributed on the carbon cloth. As the porous structure was formed in the CLs, the specific surface area is large, which is beneficial for the electrochemical reactions. In addition, sufficient pathways make contribution to mass transport. There is no obvious agglomeration of nanoparticles, providing tremendous active sites for electrochemical reactions.

4.3. General performance

Figure 3 (a) shows the performance of the passive fuel cell with a 4.0 mL of aqueous solution containing 5.0 M EG and 9.0 M KOH in the anode reservoir and a 4.0 mL of aqueous solution containing 4.0 M H_2O_2 and 1.0 M H_2SO_4 in the cathode reservoir at 60^{o}C with

pretreated Nafion 211 as the membrane. It is shown that the peak power density was 65.8 mW cm^{-2} and the OCV was 1.58 V. A significant improvement can be observed that both of the peak power density and OCV increase remarkably compared to the results shown in a previous work using oxygen as oxidant (12 mW cm^{-2} and 0.7 V) [41]. This improvement is mainly attributed to the enhanced cathode reaction kinetics, because the HPRR is a two-electron rather than four-electron transfer process [42]. Although the practical voltage is as high as 1.58 V, it is still far below the theoretical voltage (2.47 V). A general explanation was proposed by Pan et al. [33]. As the H_2O_2 can be either reduced or oxidized, a hydrogen peroxide-based fuel cell will be spontaneously established in the cathode, resulting in the mixed potential. Figure 3 (b) shows the transient discharging behavior of this passive fuel cell at a constant current density of 5 mA cm^{-2} under the same feeding concentrations but a different temperature of 23ºC. When the cell was discharging, the voltage gradually decreased because the consumption of the reactants resulted in a lower concentration gradient, thus the diffusion of the reactants to the CLs was weaker. After the voltage plateau, the voltage dramatically decreased due to the continuous drop of concentration gradient as well as the accumulation of products on the active sites. When the voltage was lower than 0.6 V, the cell was refueled with fresh anolyte and catholyte and the constant current discharging was repeated. Clearly, this fuel cell system can be stably operated for around 150 h in constant-current discharging, indicating that the potential of this passive fuel cell for practical applications.

In a passive DEGFC, the mass transport of reactants, from the fuel reservoir through the current collector holes and then the porous diffusion layer to the porous catalyst layer, is mainly driven by the concentration gradient, i.e., diffusion [43], in which the oxidation/reduction reaction will take place to consume the reactants, while the remaining will transport through the membrane reach the other electrode, wasting the utilization

efficiency of reactants and even causing the mixed potential problem [44]. In order to achieve the optimal fuel cell performance, therefore, the local concentrations of reactants in the catalyst layer should be at an appropriate level [39]. For a given design of a passive DEGFC, the reactant-feeding concentrations in the fuel reservoir are the key factor that affects the local concentrations in the catalyst layer, which means that there is an optimal reactant-feeding concentration in the fuel reservoir. Too low reactant-feeding concentration of each reactant in the fuel reservoir leads to the local concentration in the catalyst layer at an inadequate level. Too high reactant-feeding concentration of each reactant causes the high reactant crossover rate and severe competitive adsorption between two reactants on active sites, leading to the other reactant at a starvation level. Therefore, it is critically important to study the effect of the reactant-feeding concentration of each reactant in the fuel reservoir on the fuel cell performance.

4.4. Effect of the hydroxide ion concentration

Figure 4 (a) demonstrates the performance of the DEGFC running on various KOH concentrations with EG, H_2O_2, and H_2SO_4 concentrations fixed at 5.0, 4.0, and 1.0 M, respectively. Both anolyte and catholyte were of 4.0 mL, while the pretreated Nafion 211 was utilized as the membrane and the operating temperature was at 23ºC. It is seen that the OCV boosted from 1.27 V to 1.54 V with the OH^- concentration increasing from 3.0 M to 9.0 M. This improvement can be elucidated as follows. Although the performance of catalyst can be substantially improved via modification [45], for a specific catalyst of anode, the concentrations of EG and OH^- in the CL have the major effect on the kinetics of EGOR. As the EG has a constant concentration of 1.0 M, a higher KOH feeding concentration is beneficial to the hydroxide ion transport from the fuel reservoir to the anode CL, transferring it from starvation state to sufficient state. The enhanced hydroxide ion transport is derived from the higher concentration gradient of hydroxide ions, as the main driving force for

reactants to transport in passive fuel cell is diffusion. As a result, the EGOR kinetics are enhanced, which can be confirmed by the increased OCV, as shown in Figure 4 (b). However, when the concentration of OH^- was increased from 7.0 M to 9.0 M, the OCVs were similar, indicating that further increasing the OH^- concentration did not bring about higher OCV. The explanation for this phenomenon is that the adsorption of OH^- on active sites is already saturated when the OH^- concentration is 7.0 M, so the positive effect on the OCV is negligible when the OH^- concentration is 9.0 M. It is worth mentioning that the adsorption competition between OH^- and EG on active sites may lead to the starvation state of EG [46], resulting in the declined voltage. It can be seen that under 9.0 M OH^- operation, the highest peak power density was as high as 30.3 mW cm^{-2}, whereas either higher or lower OH^- concentration would cause the performance degradation. The reasons can be described as follows. In general, the electrochemical kinetics as well as the transport of species in the anode will be heavily affected by the alkalinity of the anode. On one hand, when the OH^- concentration raises from 3.0 M to 9.0 M, the internal resistance increases from 620 mOhm to 927 mOhm, as shown in Figure 4 (b). Although the ohmic loss is enhanced, the EGOR kinetics is improved, which can compensate the promoted ohmic loss, resulting in the improved performance. On the other hand, when the OH^- concentration increases from 9.0 M to 11.0 M, the internal resistance further increases to 1077 mOhm, resulting in a severer ohmic loss. It is because when the KOH concentration exceeds the optimal level, the undesired competitive adsorption between EG and OH^- occurs, resulting in the lack of EG reversely. Therefore, the active sites will be occupied and the EG adsorption will be suppressed due to too high OH^- concentration, resulting in reduced EGOR kinetics and higher concentration loss. In addition, the KOH concentration in the CL will be so high that it transports through the CEM reaching the cathode and covering the cathode active sites, thus

the HPRR is hindered due to the loss of active sites. As a result, the performance declines with OH^- concentration increasing from 9.0 M to 11.0 M.

4.5. Effect of the ethylene glycol concentration

As shown in Figure 4 (c), the effect of the concentration of EG on the cell performance was tested, where the concentrations of KOH, H_2O_2 and H_2SO_4 were fixed at 9.0 M, 4.0 M and 1.0 M, respectively. The concentration of EG was increasing from 1.0 M to 7.0 M, while the voltage of this cell over the whole range of current density exhibited an increasing trend firstly when the concentration of EG was increased from 1.0 M to 5.0 M, and then went through a decline when further increasing the concentration of EG from 5.0 M to 7.0 M. The former increasing trend of the cell voltage is attributed to the following reasons. As the concentration of EG becomes higher from 1.0 M to 5.0 M, the diffusion of EG to the actives sites on anode CL is improved, which reduces the concentration loss of EG. In Figure 4 (d), it can be seen that the OCV is elevated as the concentration of EG is increased from 1.0 M to 5.0 M as well. Meanwhile, the cell performance with the 1.0 M EG concentration exhibited a severe decline when the current density is in the range of 36 mA cm^{-2} to 37 mA cm^{-2}. With 3.0 M EG concentration, a similar decline of cell performance occurred in the current density range of 41 mA cm^{-2} to 43 mA cm^{-2}. However, no such kind of performance decline was found with higher concentration of EG, such as 5.0 M and 7.0 M. The severe decline of cell performance is attributed to the vast concentration loss as the EG concentration is low and the transport of EG to the active sites is not sufficient to support the need for the electrochemical reactions on the anode. As it is seen from Figure 4 (c), the OCV of this cell and the power output experienced a drop when increasing the concentration of EG from 5.0 M to 7.0 M. Three reasons make contributions to this noticeable drop of the cell performance. Firstly, as mentioned before, the transport of EG to the active sites is boosted with higher EG concentration. However, when its concentration reaches 7.0 M, it is actually superfluous and

brings the problem of competitive adsorption between EG and OH^-. With a high concentration of EG, the active sites on anode CL are taken up by EG, and the OH^- will be insufficient in the EGOR. Secondly, as the concentration of EG is increasing, the crossover problem of EG from the anode to cathode becomes severer. As a result, the crossover of EG enhances the mixed potential and reduces the cathode potential. The subdued electrochemical kinetics and the increased concentration loss of OH^- function together and lower the OCV of this cell. Lastly, the mass/charge transport is hindered by the increasing viscosity of anode solution with high EG concentration, which is proved by the elevated internal resistance, as shown in Figure 4 (d). The ohmic loss is enhanced due to the higher internal resistance, and thus, the cell performance is degraded.

4.6. Effect of the hydrogen peroxide concentration

As shown in Figure 5 (a), the effect of the concentration of hydrogen peroxide on the performance of this fuel cell was studied. Meanwhile, the Figure 5 (b) shows the OCVs and internal resistances of this fuel cell with different concentrations of H_2O_2, which were 2.0 M, 4.0 M, and 6.0 M. The concentrations of KOH, EG and H_2SO_4 were fixed at 9.0 M, 5.0 M and 1.0 M, respectively. The OCV decreased continuously with increasing concentration of H_2O_2. This reduction in OCV is mainly attributed to the severer crossover problem of the H_2O_2 from the cathode to anode when the H_2O_2 concentration is increased. The permeated H_2O_2 will not react with EG, producing a mixed potential, however, the H_2O_2 self-decomposition will produce gaseous oxygen, which may hinder the transport of EG and OH^- in the anode. Therefore, a lower H_2O_2 concentration results in a higher OCV. In spite of the OCV, as the concentration of H_2O_2 increased from 2.0 M to 4.0 M, the cell voltage increased over the whole range of current density and decreased subsequently when the concentration of H_2O_2 was further elevated from 4.0 M to 6.0 M, which can be explained by the following reason. From 2.0 M to 4.0 M, although the crossover problem of H_2O_2 is severer with a

higher H_2O_2 concentration, the H_2O_2 has a better transportation to the active sites on the cathode CL, which changes it to sufficient state from the starvation state. This positive effect brought by the enhanced transport of H_2O_2 compensates the negative effect brought by the crossover of H_2O_2, so that both the cell voltage and the power output are improved. However, when the concentration of H_2O_2 was increased from 4.0 M to 6.0 M, the cell voltage and power output were degraded. The reasons can be concluded as follows. Firstly, as mentioned above, the crossover problem becomes severer with higher concentration of H_2O_2, which lower the OCV. Secondly, the competitive adsorption occurs between hydrogen peroxide and protons on the active sites in cathode CL, which is brought by the superfluous H_2O_2. As a result, this problem increases the concentration loss of H^+. Lastly, the internal resistance becomes larger with higher H_2O_2 concentration, as shown in Figure 5 (b), which brings a larger ohmic loss. It can also be seen from the Figure 5 (a) that the cell performance with 6.0 M H_2O_2 exceeded that of 2.0 M H_2O_2 when the current density was high. The cell performance in this region is promoted with a higher concentration of H_2O_2, which is attributed to the reduced concentration loss of H_2O_2 in cathode.

4.7. Effect of the sulfuric acid concentration

As shown in Figure 5 (c), the effect of the concentration of sulfuric acid on the performance of this fuel cell was investigated, and the concentrations of KOH, EG and H_2O_2 were fixed at 9.0 M, 5.0 M and 4.0 M, respectively. The OCVs with different H_2SO_4 concentration were similar, as shown in Figure 5 (d). In spite of the OCV, as the concentration of H_2SO_4 increased from 0.5 M to 1.0 M, the cell voltage over the whole range of current density increased firstly. Then, further increasing the concentration of H_2SO_4 from 1.0 M to 2.0 M results in a decrease in the cell voltage. The rise of the cell voltage as the concentration of H_2SO_4 increased from 0.5 M to 1.0 M is attributed to the reduction in concentration loss of H^+, because the H^+ has an enhanced transport to the active sites on CL [47]. However, when

the H_2SO_4 concentration increased from 1.0 M to 2.0 M, the cell performance degraded, which is mainly ascribed to two reasons. On one hand, the shortage of H_2O_2 occurs because the superfluous H_2SO_4 covered the active sites on the cathode CL. The concentration loss increases because of the deficiency of H_2O_2 on the active sites, and the cell voltage decreases as a result of that. On the other hand, the ohmic loss increases due to the high concentration of H_2SO_4. The increasing concentration of H_2SO_4 gives rise to a higher viscosity of the catholyte, which increases the internal resistance in a linear manner and the ohmic loss as well. Due to these two reasons, the cell performance with 2.0 M H_2SO_4 had a serious degradation comparing to the performance with 1.0 M H_2SO_4.

4.8. Effect of the membrane thickness

The effect of membrane thickness on cell performance was studied by using different CEMs (N211, N212, and N115) at 23°C, where 4 mL aqueous solution of 5.0 M EG and 9.0 M KOH was contained in anode reservoir and 4 mL aqueous solution of 1.0 M H_2SO_4 and 4.0 M H_2O_2 was contained in cathode reservoir, and the results are shown in Figure 6 (a). When the current density was low, a thicker membrane yielded a superior cell performance, which can be confirmed by the OCVs shown in Figure 6 (b). However, the performance of this passive fuel cell was better with a thinner CEM at medium and high current densities. This phenomenon can be explained as follows. A thicker membrane suppresses the crossover of both EG from the anode to cathode and H_2O_2 from the cathode to anode. As a result, the negative effects derived from species crossover are hindered and the cell voltage increases at low current density region. However, the ohmic loss plays an important role during the discharging process, especially at medium and high current densities. As shown in Figure 6 (b), as the membrane thickness increased, the internal resistance also increased considerably, which led to a rapider degradation of the cell voltage during the whole discharging process.

As a result, the cell had a worse performance with thicker membrane due to the increasing ohmic loss at both medium and high current densities.

4.9. Effect of the operating temperature

The operating temperature of this passive fuel cell has a considerable effect on the cell performance. When the operating temperature increased, the cell performance also had an obvious improvement. The cell performance was studied with different operating temperatures as shown in Figure 7, where 4 mL aqueous solution of 5.0 M EG and 9.0 M KOH was contained in anode reservoir and 4 mL aqueous solution of 1.0 M H_2SO_4 and 4.0 M H_2O_2 was contained in cathode reservoir, and the pretreated Nafion 211 was utilized as the membrane. When the operating temperatures of this fuel cell were at 23ºC, 40ºC, and 60ºC, the peak power densities reached 30.3, 39.6 and 65.8 mW cm^{-2}, respectively. The impressive enhancement in cell performance is attributed to three reasons. Firstly, the increasing temperature promotes the kinetics of both anode and cathode reactions, including the EGOR and HPRR, which decreases the activation loss during the discharging process [48]. Secondly, the concentration loss decreases with increasing operating temperature. The transport of the reactants in both anolyte and catholyte is improved with higher temperature. The transport of cations through the membrane is boosted as well. As a result of this enhanced transport, the reactants reach the active sites on the CLs more easily, thus the concentration loss decreases because of the alleviative reactant shortage. Lastly, as the operating temperature increases, the CEMs will have a better conductivity, which brings a reduction in ohmic loss. The three improvements result in a better performance of this fuel cell.

4.10. Effect of the hydrogen peroxide self-decomposition

As mentioned, the H_2O_2 self-decomposition will take place in the cathode, and it is an exothermic reaction according to:

$$2H_2O_2 \rightarrow O_2 + 2H_2O \qquad \Delta H = -196.1 \text{ kJ mol}^{-1}$$

Meanwhile, both the electrochemical reactions on the anode and the cathode are exothermic reactions as well, so the cell temperature will increase during discharging. Therefore, it is critical to determine whether the heat released from the H_2O_2 self-decomposition plays an important role in the cell temperature. If the cell temperature increases rapidly due to the H_2O_2 self-decomposition, it is necessary to adopt heat management methods to control the cell temperature at a reasonable range. Figure 8 shows the transient temperature behaviors of the passive fuel cell under 20, 40, and 80 mA constant current discharging operation, where 4 mL aqueous solution of 5.0 M EG and 9.0 M KOH was contained in anode reservoir and 4 mL aqueous solution of 1.0 M H_2SO_4 and 4.0 M H_2O_2 was contained in cathode reservoir, and the pretreated Nafion 211 was utilized as the membrane at 23°C. It can be seen that the cell temperature first increased from the room temperature, 23°C, with the discharging time, and finally reached a stable temperature, indicating the heat balance between the cell and external environment. The increased temperatures were 0.5, 1.1, and 2.0°C under 20, 40, and 80 mA current discharging operation, respectively. It can be inferred from the linear temperature increase with the discharging current that the increased temperature is caused by the electrochemical reactions rather than the H_2O_2 self-decomposition. Otherwise, the increased temperature at three different discharging currents should be similar rather than the linear increase. Therefore, both the electrochemical reactions on the anode and the cathode play the dominant role in the cell temperature.

5. Concluding remarks

A passive direct ethylene glycol fuel cell is proposed and tested in this work. Different operating conditions are tested to investigate the effects of different feeding concentrations of reactants, different thicknesses of the cation exchange membranes, and different operating temperatures on the cell performance. The results exhibit that the peak power densities of this fuel cell are 30.3 and 65.8 mW cm^{-2} at 23 and 60°C, respectively, with optimal aqueous

anolyte containing 5.0 M EG and 9.0 M KOH, and optimal aqueous catholyte containing 1.0 M H_2SO_4 and 4.0 M H_2O_2. In addition, the results show that the thickness of the CEMs has a significant effect on cell performance. Although a thicker membrane reduces the crossover problem, a thinner one shows a significant reduction in ohmic loss, resulting in a superior cell performance. As a result, the cation exchange membrane prepared from N211 exhibits the best performance. The performance of this fuel cell under the optimal operating conditions (1.58 V and 65.8 mW cm^{-2}) has an impressive improvement comparing to a passive direct ethylene glycol fuel cell with oxygen as oxidant, which is more than 2 times in the open circuit voltage and more than 5 times in the peak power density. The excellent performance is mainly attributed to the faster kinetics of hydrogen peroxide reduction reaction due to the two-electron-transfer process. Moreover, the effect of the heat released by the self-decomposition of hydrogen peroxide is also investigated. The results indicate that the hydrogen peroxide self-decomposition shows a negligible effect on the total heat released over the discharging process, during which both the electrochemical reactions on the anode and cathode play the dominant role.

Acknowledgement:

This work was fully supported by a grant from the Research Grants Council of the Hong Kong Special Administrative Region, China (Project No. 25211817).

References

[1] Pan ZF, An L, Zhao TS, Tang ZK. Advances and challenges in alkaline anion exchange membrane fuel cells. Progress in Energy and Combustion Science 2018;66:141-75.

[2] An L, Zhao T. Anion exchange membrane fuel cells: principles, materials and systems: Springer; 2018.

[3] Wu QX, Pan ZF, An L. Recent advances in alkali-doped polybenzimidazole membranes for fuel cell applications. Renewable and Sustainable Energy Reviews 2018;89:168-83.

[4] Pan ZF, An L, Wen CY. Recent advances in fuel cells based propulsion systems for unmanned aerial vehicles. Applied Energy 2019;240:473-85.

[5] Mahato N, Banerjee A, Gupta A, Omar S, Balani K. Progress in material selection for solid oxide fuel cell technology: A review. Progress in Materials Science 2015;72:141-337.

[6] Kulkarni A, Siahrostami S, Patel A, Nørskov JK. Understanding Catalytic Activity Trends in the Oxygen Reduction Reaction. Chemical Reviews 2018;118:2302-12.

[7] Gewirth AA, Varnell JA, DiAscro AM. Nonprecious Metal Catalysts for Oxygen Reduction in Heterogeneous Aqueous Systems. Chemical Reviews 2018;118:2313-39.

[8] Li Y, Sun X, Feng Y. Hydroxide Self-Feeding High-Temperature Alkaline Direct Formate Fuel Cells. ChemSusChem 2017;10:2135-9.

[9] Wen C-Y, Lin Y-S, Lu C-H. Performance of a proton exchange membrane fuel cell stack with thermally conductive pyrolytic graphite sheets for thermal management. Journal of Power Sources 2009;189:1100-5.

[10] Zhao TS, Xu C, Chen R, Yang WW. Mass transport phenomena in direct methanol fuel cells. Progress in Energy and Combustion Science 2009;35:275-92.

[11] An L, Zhao TS. Transport phenomena in alkaline direct ethanol fuel cells for sustainable energy production. Journal of Power Sources 2017;341:199-211.

[12] Wang C, Mo B, He Z, Shao Q, Pan D, Wujick E, Guo J, Xie X, Xie X, Guo Z. Crosslinked norbornene copolymer anion exchange membrane for fuel cells. Journal of Membrane Science 2018;556:118-25.

[13] An L, Chen R. Mathematical modeling of direct formate fuel cells. Applied Thermal Engineering 2017;124:232-40.

[14] Omasta TJ, Wang L, Peng X, Lewis CA, Varcoe JR, Mustain WE. Importance of balancing membrane and electrode water in anion exchange membrane fuel cells. Journal of Power Sources 2018;375:205-13.

[15] Li Y, He Y, Yang W. A high-performance direct formate-peroxide fuel cell with palladium–gold alloy coated foam electrodes. Journal of Power Sources 2015;278:569-73.

[16] Pan ZF, Chen R, An L, Li YS. Alkaline anion exchange membrane fuel cells for cogeneration of electricity and valuable chemicals. Journal of Power Sources 2017;365:430-45.

[17] Chen X, Li T, Shen J, Hu Z. From structures, packaging to application: A system-level review for micro direct methanol fuel cell. Renewable and Sustainable Energy Reviews 2017;80:669-78.

[18] An L, Chen R. Recent progress in alkaline direct ethylene glycol fuel cells for sustainable energy production. Journal of Power Sources 2016;329:484-501.

[19] Yue H, Zhao Y, Ma X, Gong J. Ethylene glycol: properties, synthesis, and applications. Chemical Society Reviews 2012;41:4218-44.

[20] Zhu X-Y, Zhang L, Yuan P-X, Feng J-J, Yuan J, Zhang Q-L, Wang A-J. Hollow $Ag_{44}Pt_{56}$ nanotube bundles with high electrocatalytic performances for hydrogen evolution and ethylene glycol oxidation reactions. Journal of Colloid and Interface Science 2018;532:571-8.

[21] Shi Y-C, Feng J-J, Lin X-X, Zhang L, Yuan J, Zhang Q-L, Wang A-J. One-step hydrothermal synthesis of three-dimensional nitrogen-doped reduced graphene oxide hydrogels anchored PtPd alloyed nanoparticles for ethylene glycol oxidation and hydrogen evolution reactions. Electrochimica Acta 2019;293:504-13.

[22] Huang X-Y, Wang A-J, Zhang X-F, Zhang L, Feng J-J. One-Step Synthesis of PtCu Alloyed Nanocages with Highly Open Structures as Bifunctional Electrocatalysts for Oxygen

Reduction and Polyhydric Alcohol Oxidation. ACS Applied Energy Materials 2018;1:5779-86.

[23] Pan Z, Bi Y, An L. Mathematical modeling of direct ethylene glycol fuel cells incorporating the effect of the competitive adsorption. Applied Thermal Engineering 2019;147:1115-24.

[24] An L, Zhao TS, Shen SY, Wu QX, Chen R. Performance of a direct ethylene glycol fuel cell with an anion-exchange membrane. International Journal of Hydrogen Energy 2010;35:4329-35.

[25] An L, Zeng L, Zhao TS. An alkaline direct ethylene glycol fuel cell with an alkali-doped polybenzimidazole membrane. International Journal of Hydrogen Energy 2013;38:10602-6.

[26] Wen C-Y, Lin Y-S, Lu C-H, Luo T-W. Thermal management of a proton exchange membrane fuel cell stack with pyrolytic graphite sheets and fans combined. International Journal of Hydrogen Energy 2011;36:6082-9.

[27] An L, Zhao T, Yan X, Zhou X, Tan P. The dual role of hydrogen peroxide in fuel cells. Science Bulletin 2015;60:55-64.

[28] Yu EH, Krewer U, Scott K. Principles and Materials Aspects of Direct Alkaline Alcohol Fuel Cells. Energies 2010;3.

[29] McLean GF, Niet T, Prince-Richard S, Djilali N. An assessment of alkaline fuel cell technology. International Journal of Hydrogen Energy 2002;27:507-26.

[30] An L, Zhao TS, Chai ZH, Zeng L, Tan P. Modeling of the mixed potential in hydrogen peroxide-based fuel cells. International Journal of Hydrogen Energy 2014;39:7407-16.

[31] An L, Jung CY. Transport phenomena in direct borohydride fuel cells. Applied Energy 2017;205:1270-82.

[32] Fukuzumi S, Yamada Y. Hydrogen Peroxide used as a Solar Fuel in One-Compartment Fuel Cells. ChemElectroChem 2016;3:1978-89.

[33] Pan Z, Huang B, An L. Performance of a hybrid direct ethylene glycol fuel cell. International Journal of Energy Research 2018;1-9. (https://doi.org/10.1002/er.4176)

[34] Chen W, Yuan W, Ye G, Han F, Tang Y. Utilization and positive effects of produced CO2 on the performance of a passive direct methanol fuel cell with a composite anode structure. International Journal of Hydrogen Energy 2017;42:15613-22.

[35] An L, Zhao TS, Chen R, Wu QX. A novel direct ethanol fuel cell with high power density. Journal of Power Sources 2011;196:6219-22.

[36] An L, Zhao TS. Performance of an alkaline-acid direct ethanol fuel cell. International Journal of Hydrogen Energy 2011;36:9994-9.

[37] Chen R, Zhao TS. Porous current collectors for passive direct methanol fuel cells. Electrochimica Acta 2007;52:4317-24.

[38] Chen R, Zhao TS. Performance characterization of passive direct methanol fuel cells. Journal of Power Sources 2007;167:455-60.

[39] Zhao TS, Chen R, Yang WW, Xu C. Small direct methanol fuel cells with passive supply of reactants. Journal of Power Sources 2009;191:185-202.

[40] Liu JG, Zhao TS, Chen R, Wong CW. The effect of methanol concentration on the performance of a passive DMFC. Electrochemistry Communications 2005;7:288-94.

[41] Marchionni A, Bevilacqua M, Bianchini C, Chen Y-X, Filippi J, Fornasiero P, Lavacchi A, Miller H, Wang L, Vizza F. Electrooxidation of Ethylene Glycol and Glycerol on Pd-(Ni-Zn)/C Anodes in Direct Alcohol Fuel Cells. ChemSusChem 2013;6:518-28.

[42] Miley GH, Luo N, Mather J, Burton R, Hawkins G, Gu L, Byrd E, Gimlin R, Shrestha PJ, Benavides G, Laystrom J, Carroll D. Direct NaBH4/H2O2 fuel cells. Journal of Power Sources 2007;165:509-16.

[43] Bae B, Kho BK, Lim T-H, Oh I-H, Hong S-A, Ha HY. Performance evaluation of passive DMFC single cells. Journal of Power Sources 2006;158:1256-61.

[44] Liu JG, Zhao TS, Liang ZX, Chen R. Effect of membrane thickness on the performance and efficiency of passive direct methanol fuel cells. Journal of Power Sources 2006;153:61-7.

[45] Yu Y, Yang X, Zhao Y, Zhang X, An L, Huang M, Chen G, Zhang R. Engineering the Band Gap States of the Rutile TiO2(110) Surface by Modulating the Active Heteroatom. Angewandte Chemie 2018;130:8686-90.

[46] Li YS, Zhao TS, Liang ZX. Performance of alkaline electrolyte-membrane-based direct ethanol fuel cells. Journal of Power Sources 2009;187:387-92.

[47] Raman RK, Choudhury NA, Shukla AK. A High Output Voltage Direct Borohydride Fuel Cell. Electrochemical and Solid-State Letters 2004;7:A488-A91.

[48] Li YS, Zhao TS. A high-performance integrated electrode for anion-exchange membrane direct ethanol fuel cells. International Journal of Hydrogen Energy 2011;36:7707-13.

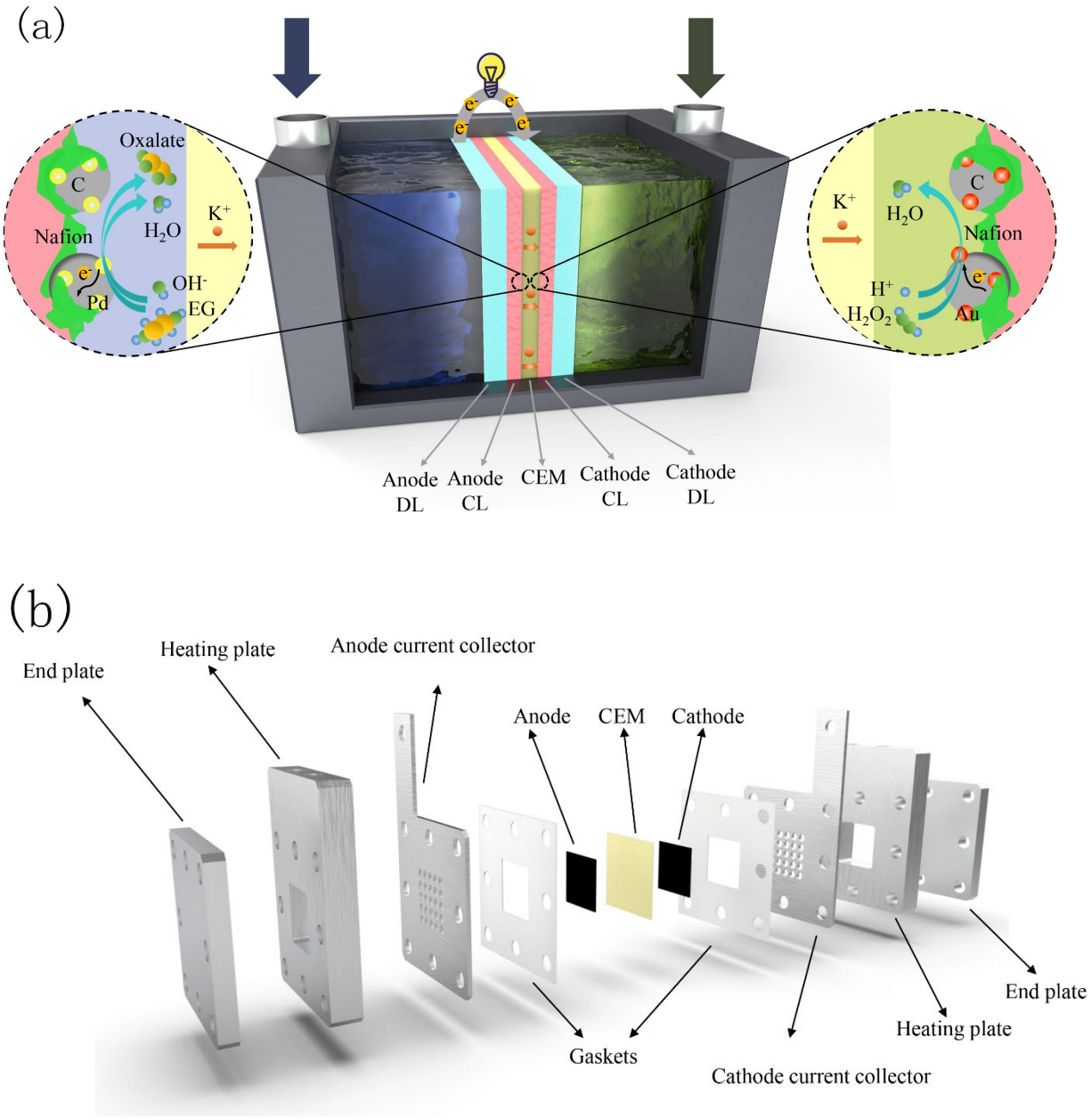
(a)
Oxalate
C
Nafion
H_2O
K^+
OH^-
EG
Pd
e^-
H^+
H_2O_2
Au
Anode DL
Anode CL
CEM
Cathode CL
Cathode DL
(b)
End plate
Heating plate
Anode current collector
Anode
CEM
Cathode
Gaskets
Cathode current collector
Heating plate
End plate

Figure 1

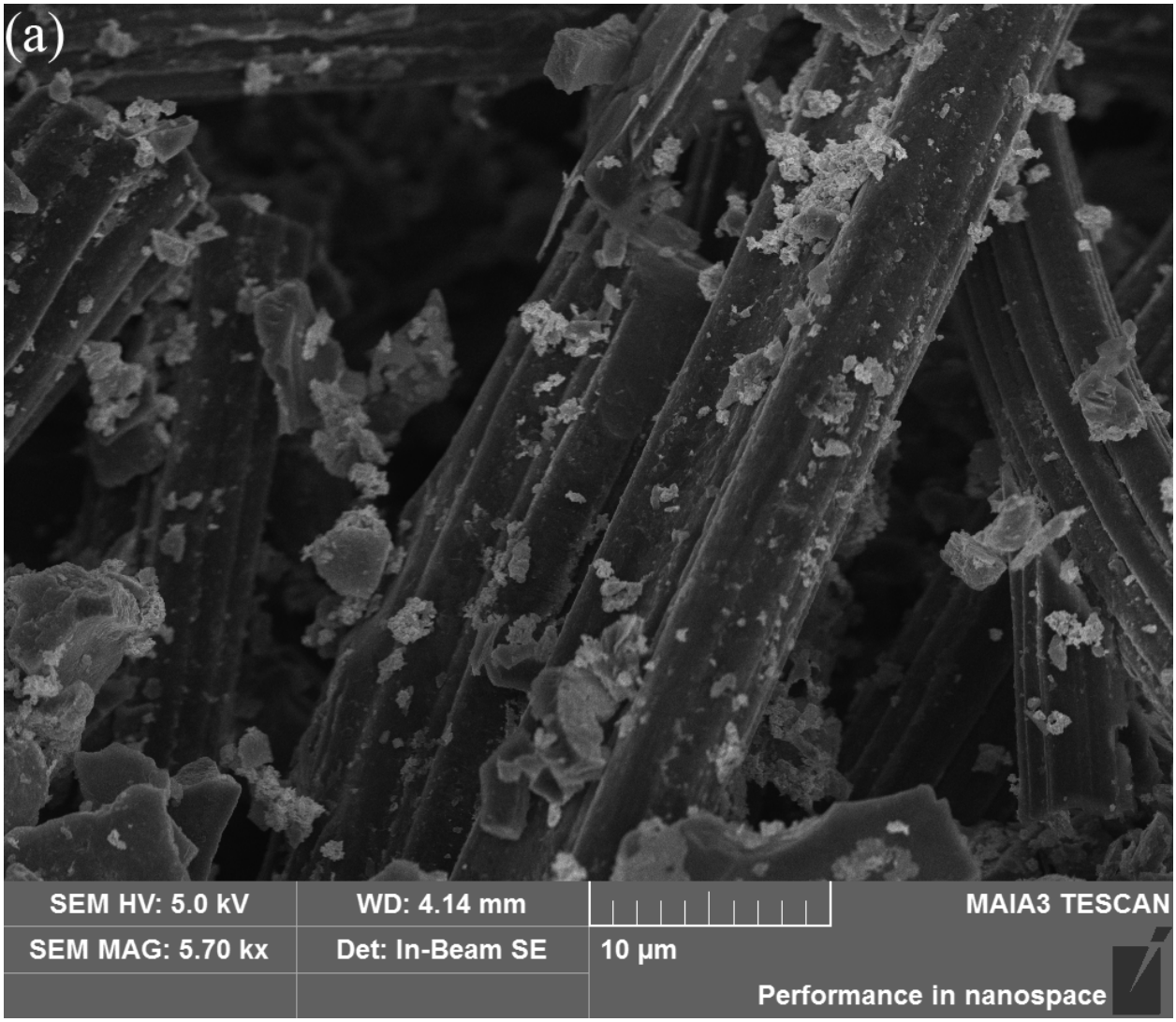
(a)
SEM HV: 5.0 kV
WD: 4.14 mm
MAIA3 TESCAN
SEM MAG: 5.70 kx
Det: In-Beam SE
10 µm
Performance in nanospace

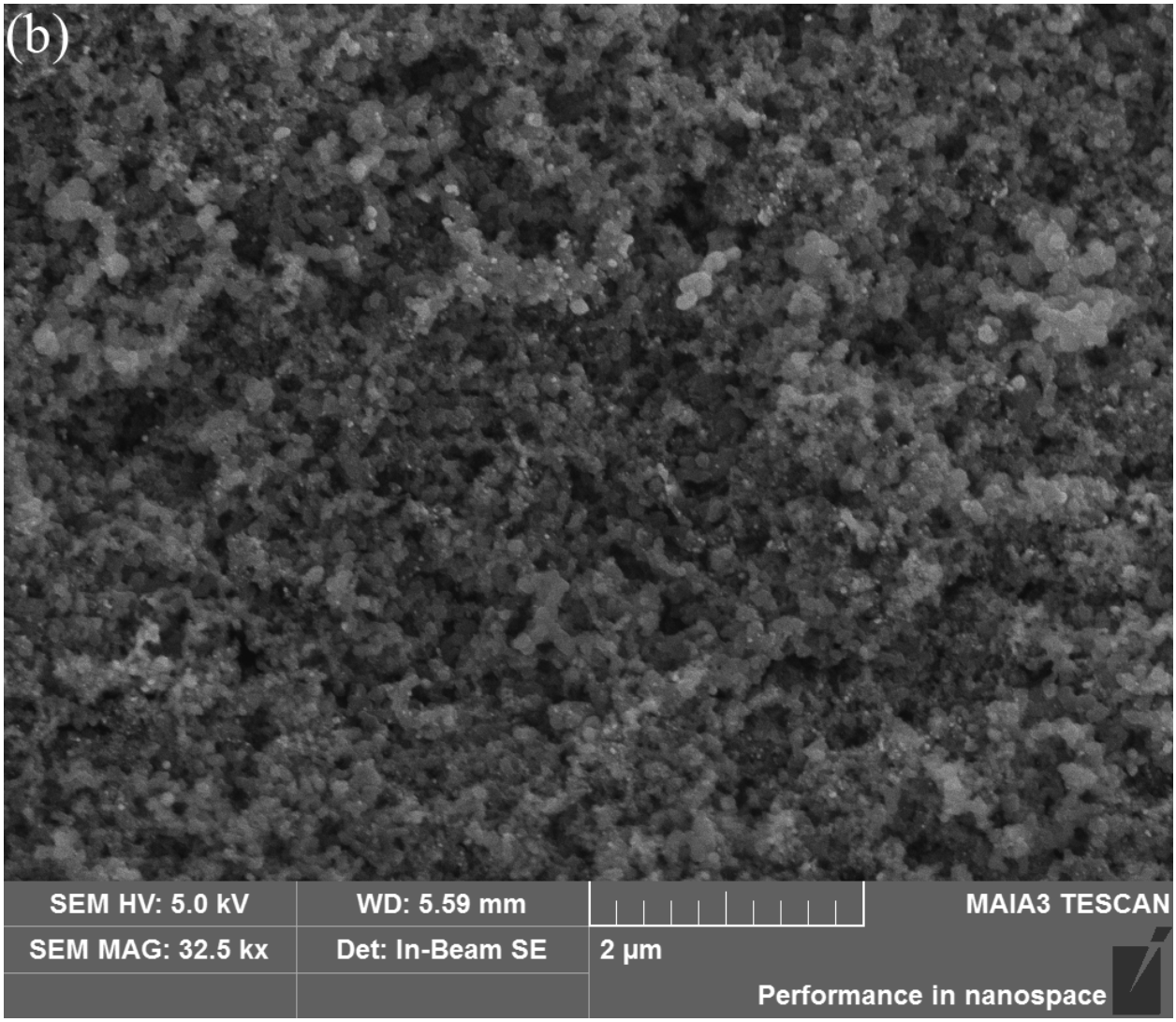
(b)
SEM HV: 5.0 kV
WD: 5.59 mm
MAIA3 TESCAN
SEM MAG: 32.5 kx
Det: In-Beam SE
2 µm
Performance in nanospace

Figure 2

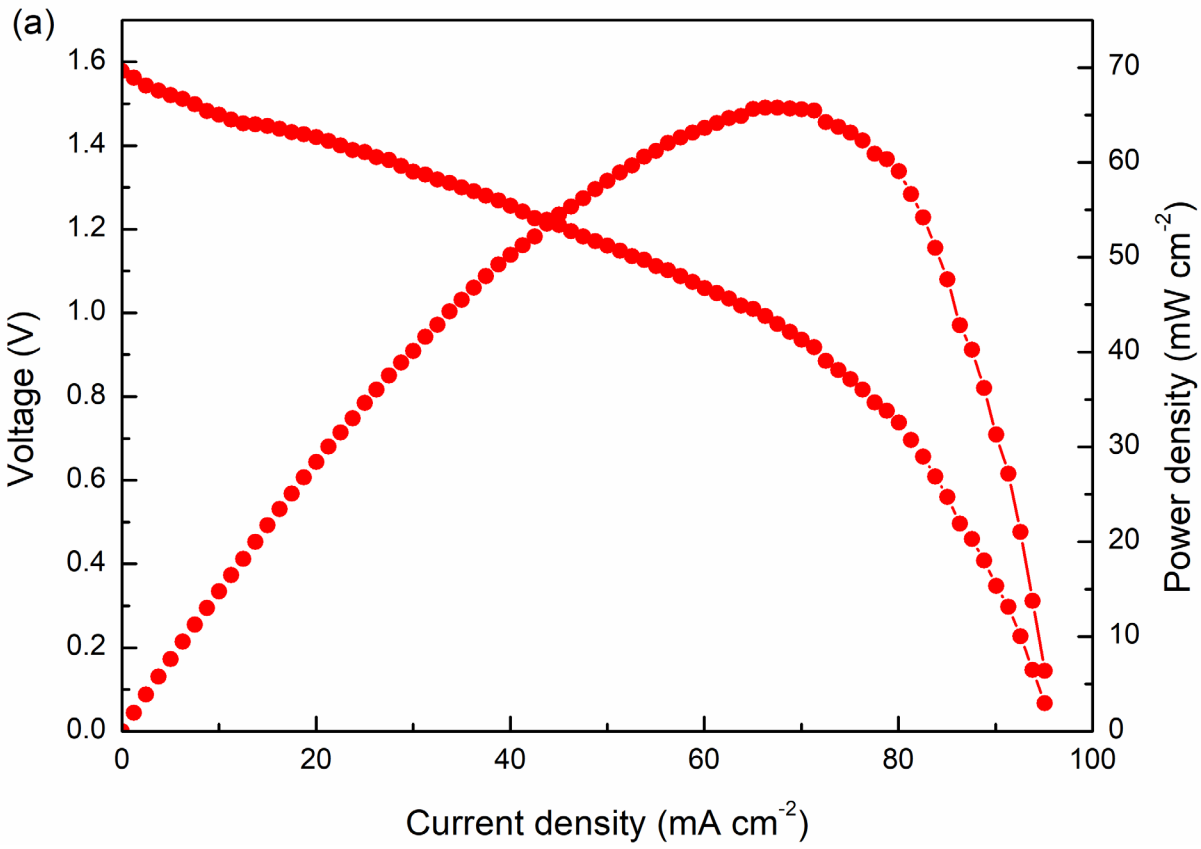
(a)
Voltage (V)
Power density (mW cm-2)
Current density (mA cm-2)
0.0
0.2
0.4
0.6
0.8
1.0
1.2
1.4
1.6
0
10
20
30
40
50
60
70
0
20
40
60
80
100

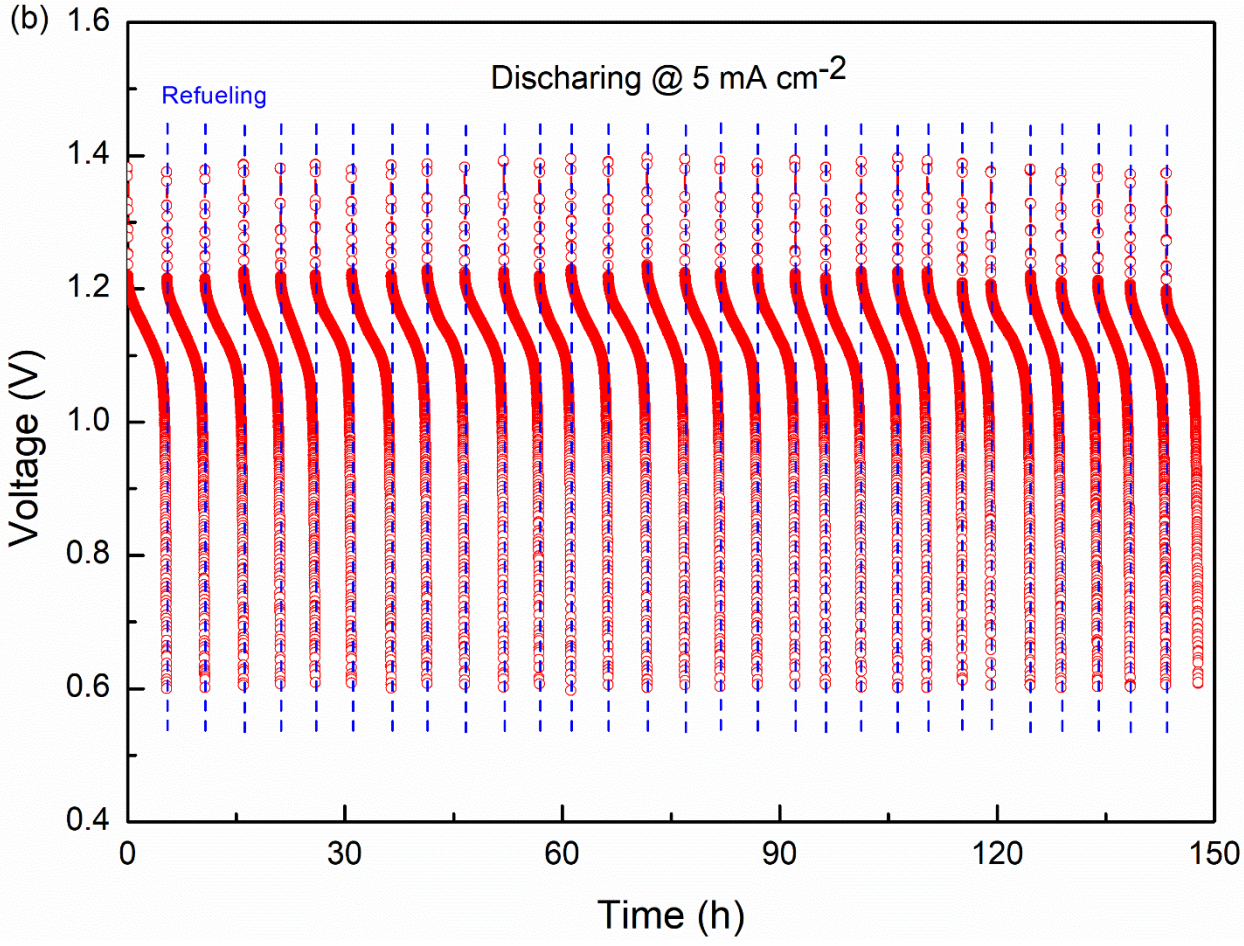
(b)
Refueling
Discharing @ 5 mA cm-2
Voltage (V)
Time (h)
0.4
0.6
0.8
1.0
1.2
1.4
1.6
0
30
60
90
120
150

Figure 3

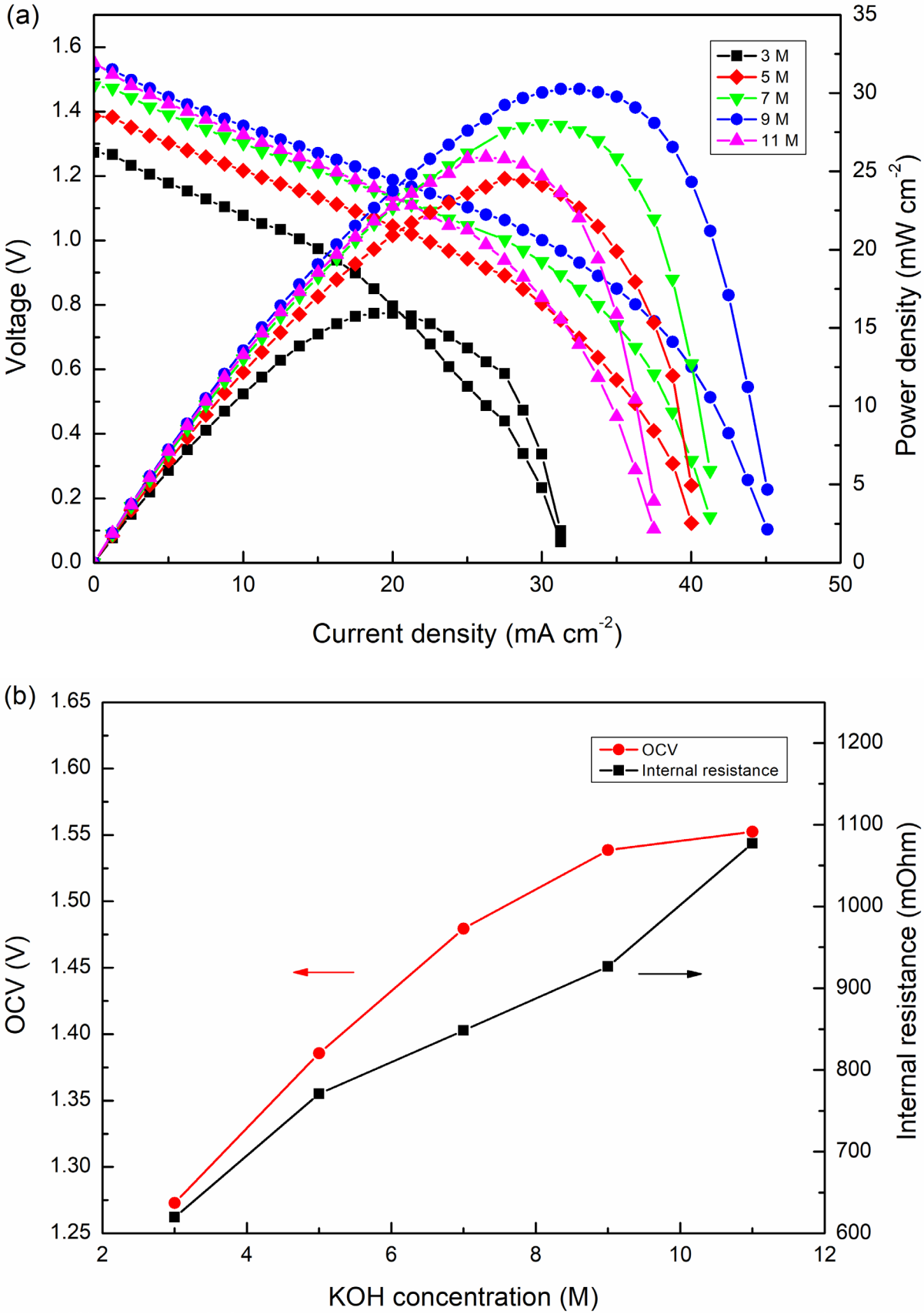
(a)
Voltage (V)
Power density (mW cm-2)
Current density (mA cm-2)
3 M
5 M
7 M
9 M
11 M
(b)
OCV (V)
Internal resistance (mOhm)
KOH concentration (M)
OCV
Internal resistance

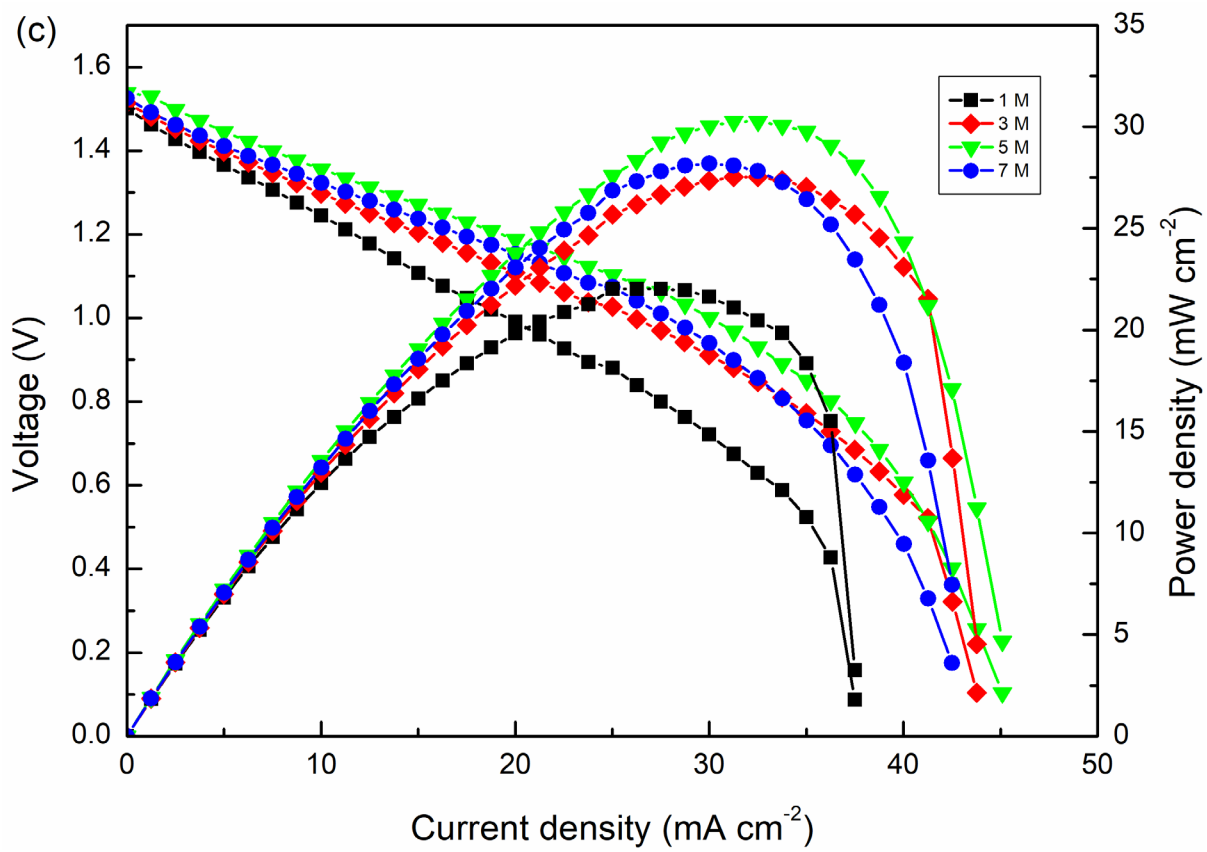
(c)
1 M
3 M
5 M
7 M
Voltage (V)
Power density (mW cm-2)
Current density (mA cm-2)
0.0
0.2
0.4
0.6
0.8
1.0
1.2
1.4
1.6
0
5
10
15
20
25
30
35
0
10
20
30
40
50

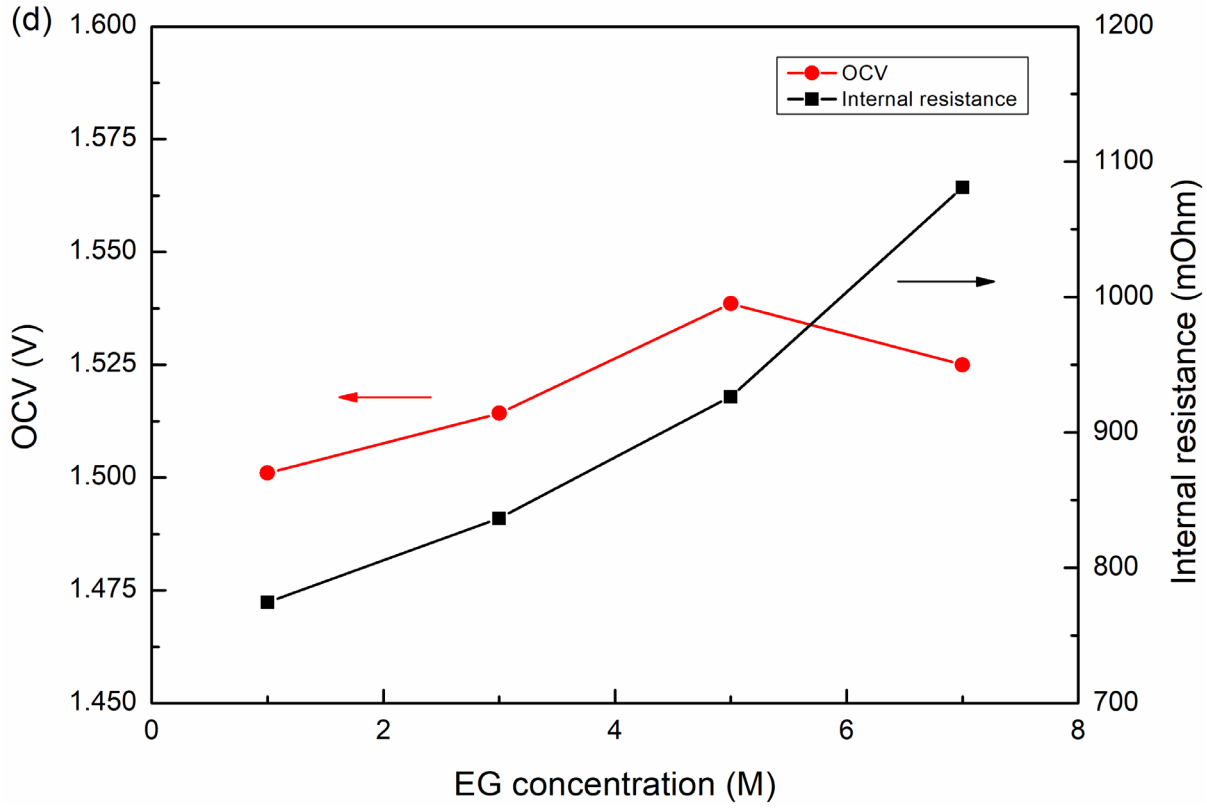
(d)
OCV
Internal resistance
OCV (V)
Internal resistance (mOhm)
EG concentration (M)
1.450
1.475
1.500
1.525
1.550
1.575
1.600
700
800
900
1000
1100
1200
0
2
4
6
8

Figure 4

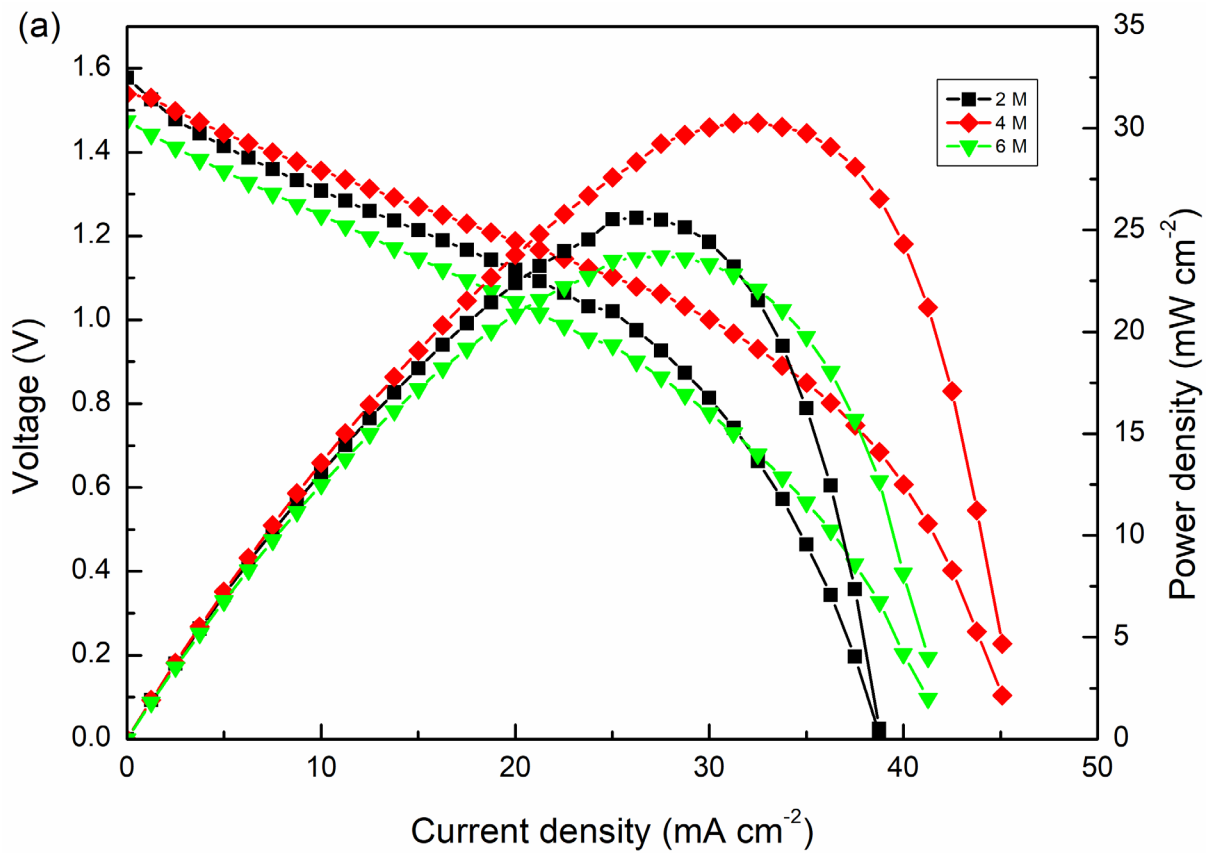
(a)
2 M
4 M
6 M
Voltage (V)
Power density (mW cm-2)
Current density (mA cm-2)
0.0
0.2
0.4
0.6
0.8
1.0
1.2
1.4
1.6
0
5
10
15
20
25
30
35
0
10
20
30
40
50

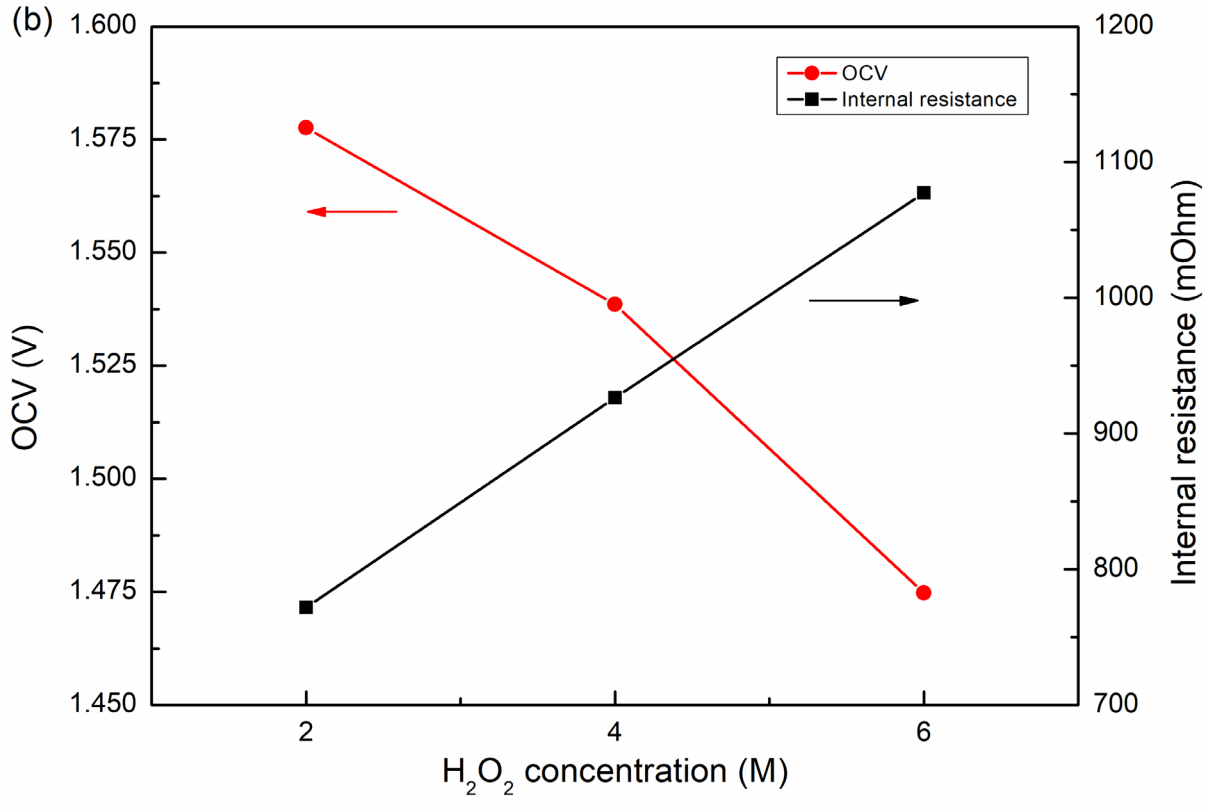
(b)
OCV
Internal resistance
OCV (V)
Internal resistance (mOhm)
H2O2 concentration (M)
1.450
1.475
1.500
1.525
1.550
1.575
1.600
700
800
900
1000
1100
1200
2
4
6

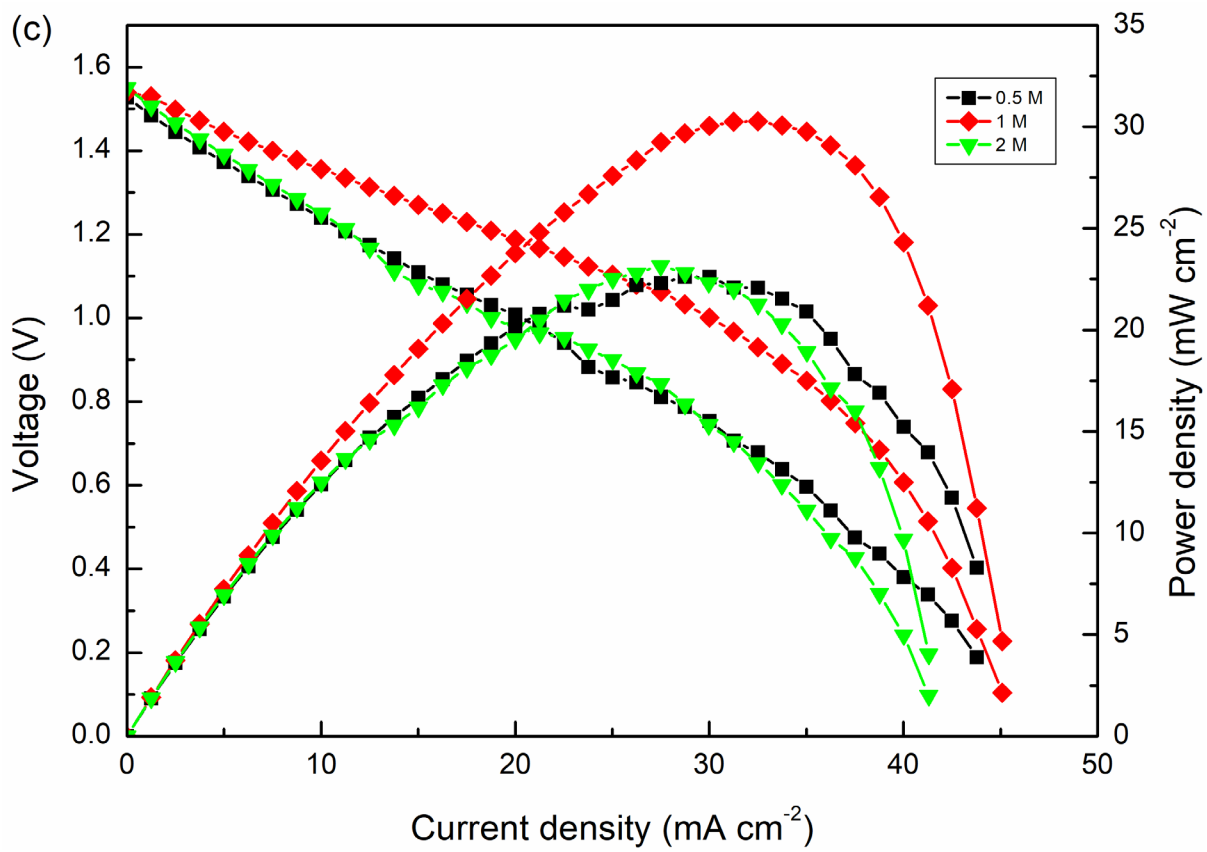
(c)
0.5 M
1 M
2 M
Voltage (V)
Power density (mW cm-2)
Current density (mA cm-2)
0.0
0.2
0.4
0.6
0.8
1.0
1.2
1.4
1.6
0
5
10
15
20
25
30
35
0
10
20
30
40
50

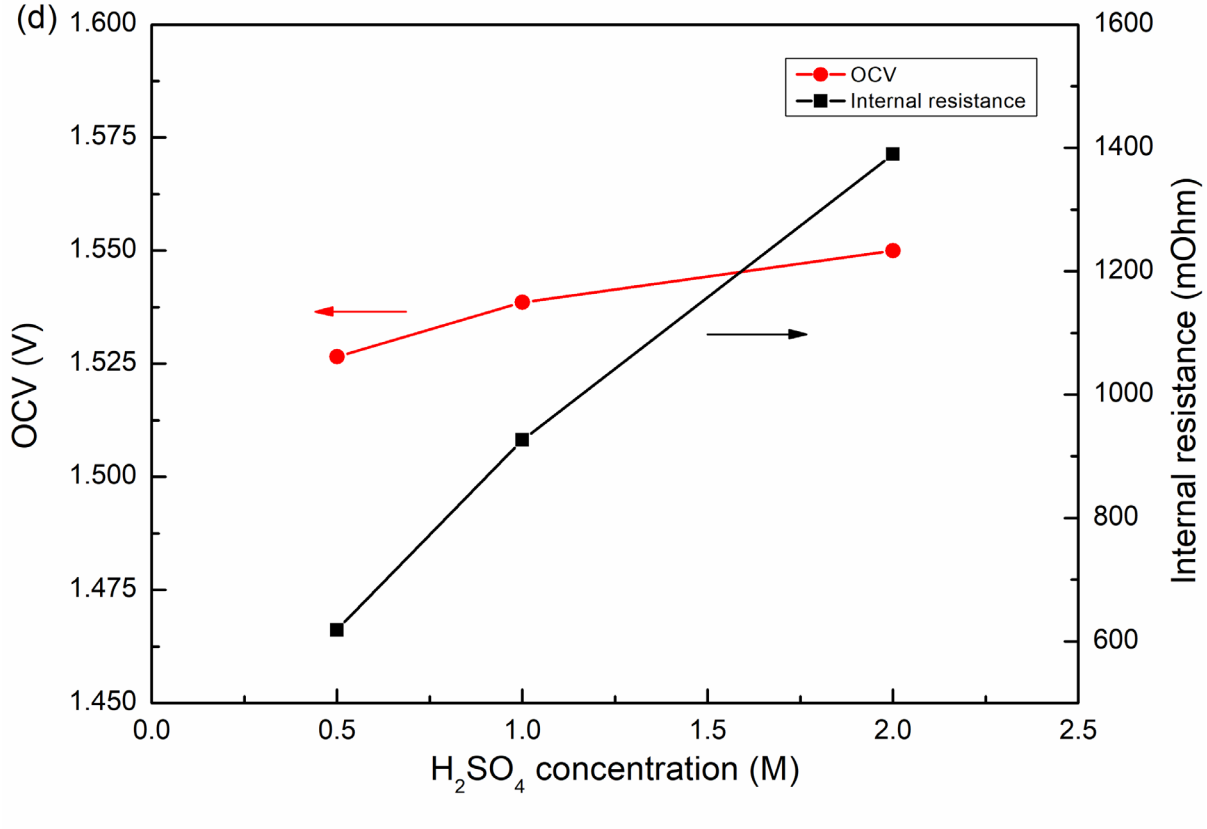
(d)
OCV
Internal resistance
OCV (V)
Internal resistance (mOhm)
H2SO4 concentration (M)
1.450
1.475
1.500
1.525
1.550
1.575
1.600
600
800
1000
1200
1400
1600
0.0
0.5
1.0
1.5
2.0
2.5

Figure 5

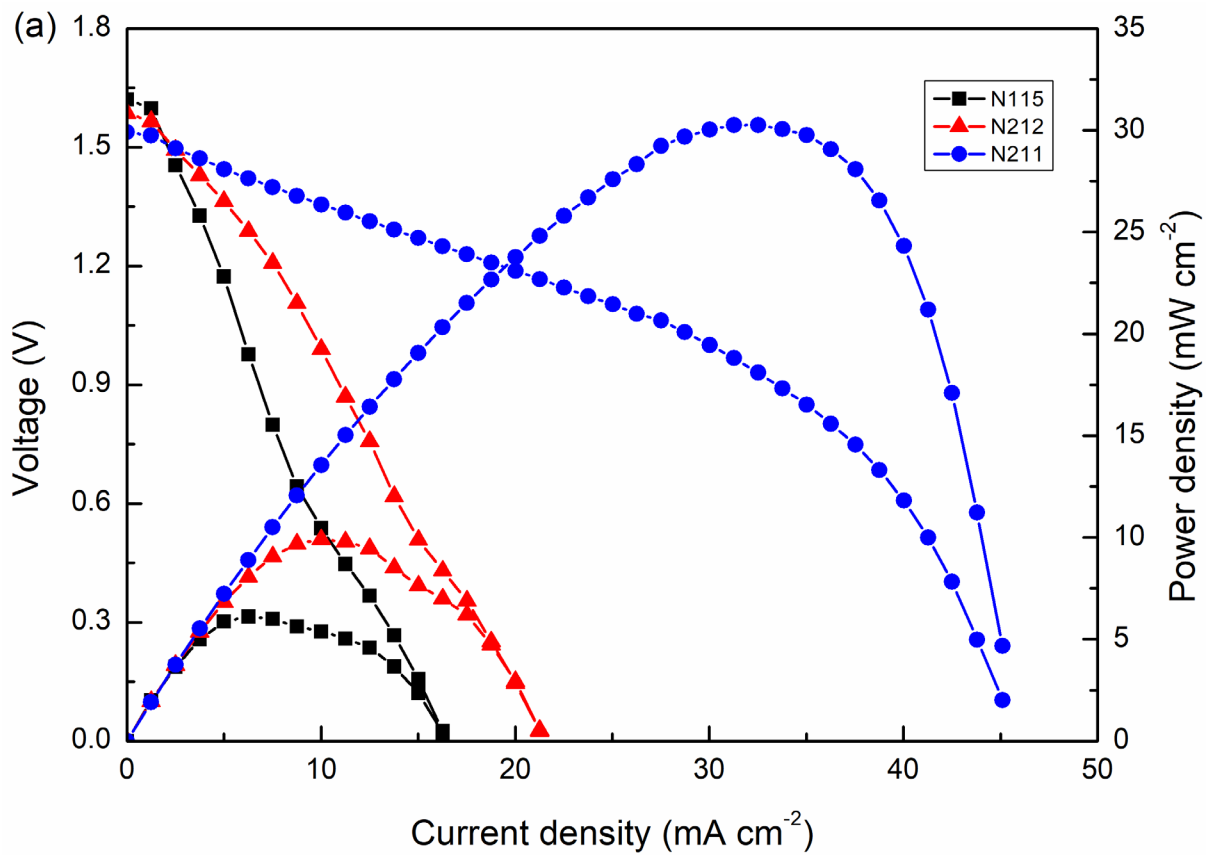
(a)
N115
N212
N211
Voltage (V)
Power density (mW cm-2)
Current density (mA cm-2)
0.0
0.3
0.6
0.9
1.2
1.5
1.8
0
5
10
15
20
25
30
35
0
10
20
30
40
50

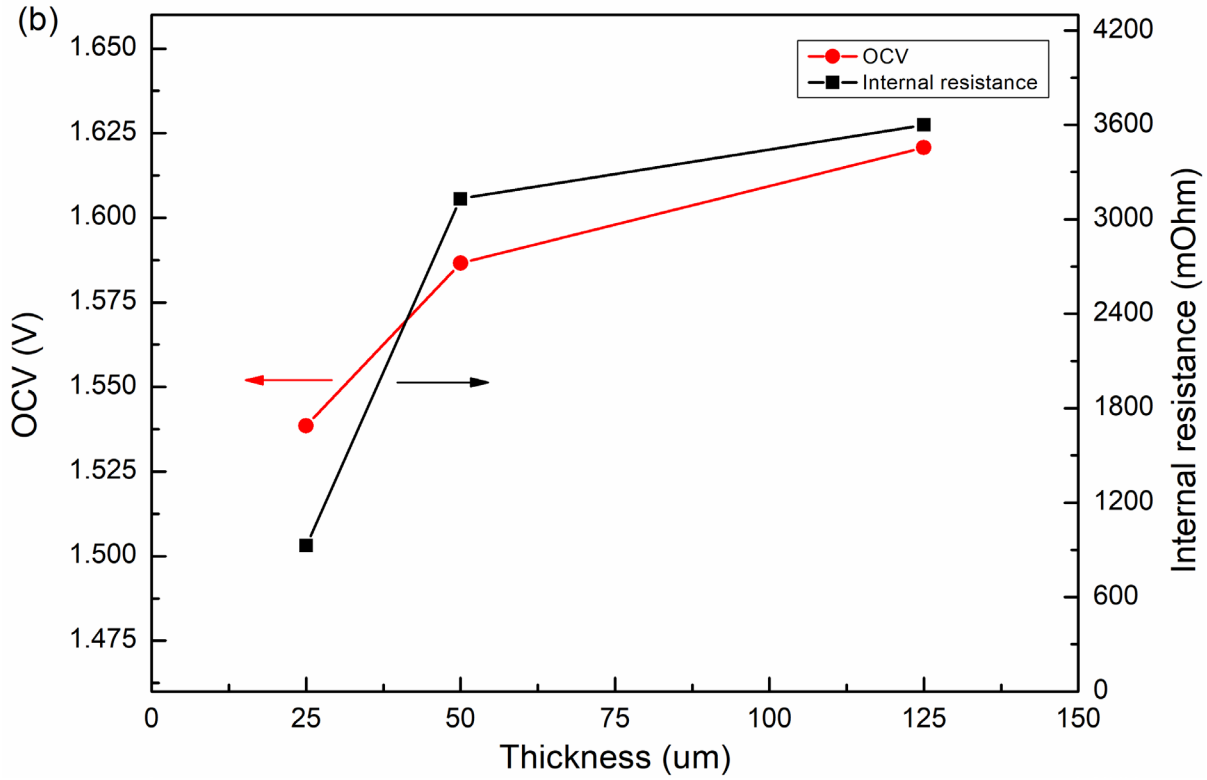
(b)
OCV
Internal resistance
OCV (V)
Internal resistance (mOhm)
Thickness (um)
1.475
1.500
1.525
1.550
1.575
1.600
1.625
1.650
0
600
1200
1800
2400
3000
3600
4200
0
25
50
75
100
125
150

Figure 6

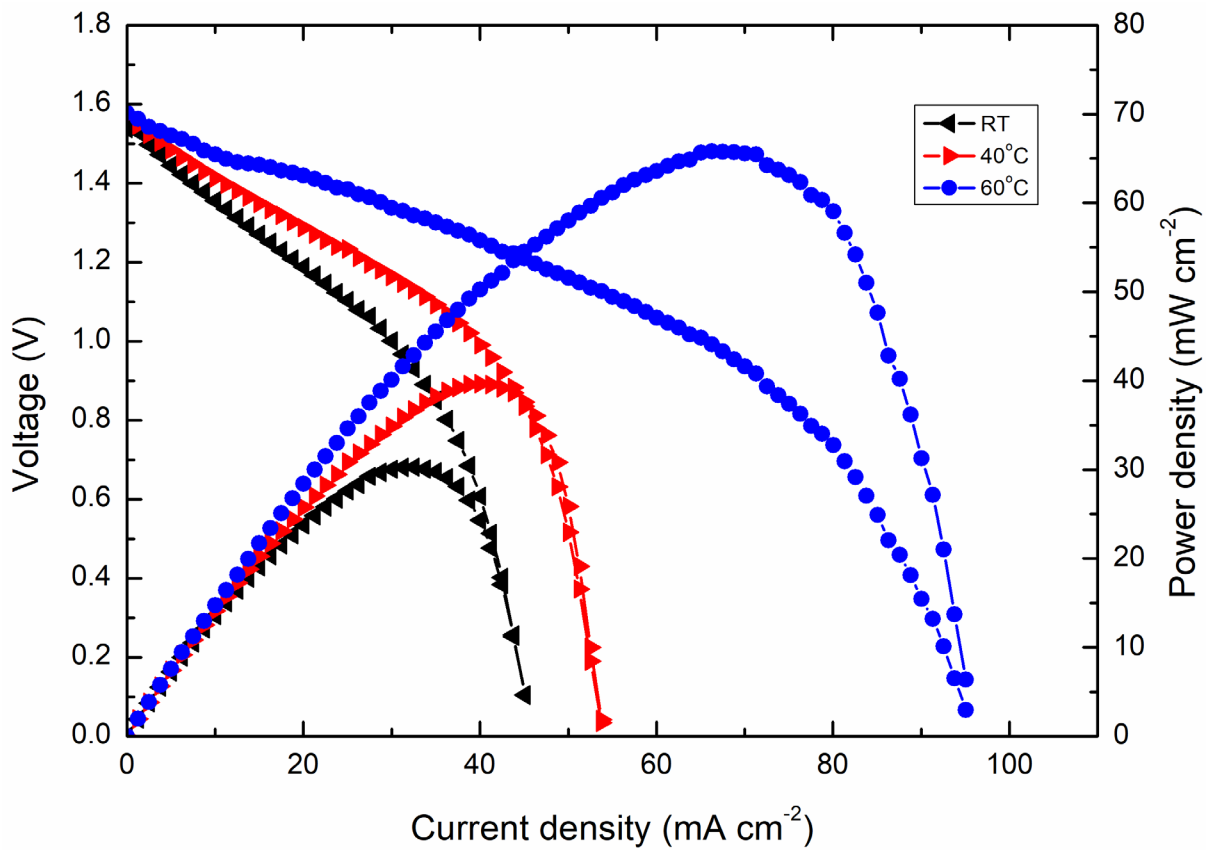
Voltage (V)
Power density (mW cm^{-2})
Current density (mA cm^{-2})
RT
40°C
60°C
0.0
0.2
0.4
0.6
0.8
1.0
1.2
1.4
1.6
1.8
0
10
20
30
40
50
60
70
80
0
20
40
60
80
100

Figure 7

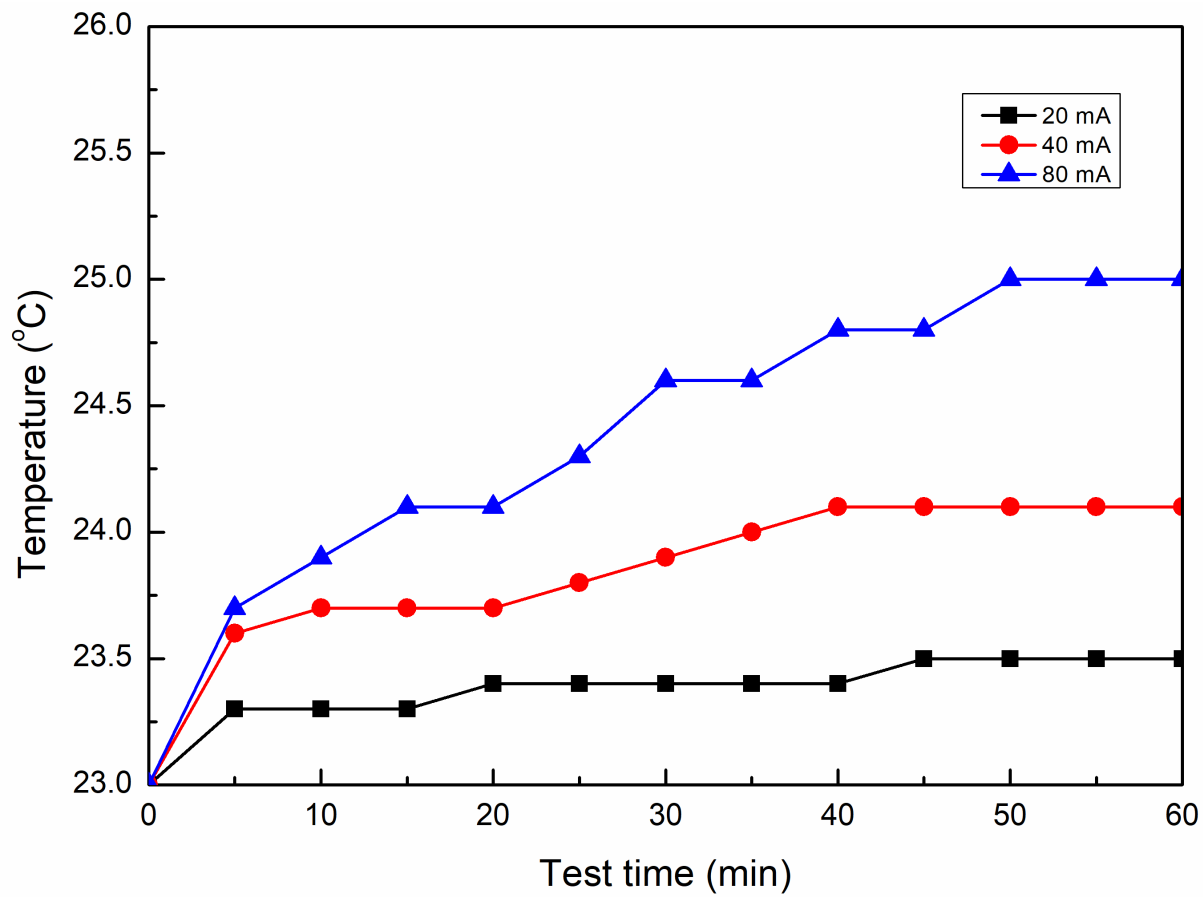

Figure 8

Figure captions:

Figure 1 (a) Working principle and (b) schematic illustration of a passive DEGFC.

Figure 2 SEM images of the catalyst layer of (a) anode and (b) cathode.

Figure 3 (a) Performance of the passive DEGFC and (b) transient discharging behavior with refueling.

Figure 4 Effect of the KOH concentration on (a) the cell performance and (b) OCV and internal resistance. Effect of the EG concentration on (c) the cell performance and (d) OCV and internal resistance.

Figure 5 Effect of the H_2O_2 concentration on (a) the cell performance and (b) OCV and internal resistance. Effect of the H_2SO_4 concentration on (c) the cell performance and (d) OCV and internal resistance.

Figure 6 Effect of the membrane thickness on (a) the cell performance and (b) OCV and internal resistance.

Figure 7 Effect of the operating temperature on the cell performance.

Figure 8 Transient cell temperature behaviors with constant current discharging.